CHAPTER III
IMPROVED METHANE HYDRATE FORMATION RATE USING TREATED ACTIVATED CARBON AND TETRAHYDROFURAN

3.1 Abstract

Effects of H_2SO_4 and KOH treated activated carbon and tetrahydrofuran (THF) on methane hydrate formation kinetics were investigated in a fixed volume crystallizer at 6 and 8 MPa and 277.15 K. The addition of the untreated activated carbon enhanced the kinetics of the hydrate formation at 8 MPa, while adding the carbon treated by H_2SO_4 and KOH increased the gas consumption during the hydrate formation and its kinetics at 6 MPa. Similarly, the presence of THF also enhanced the hydrate formation kinetics at the low pressure (6 MPa). Moreover, the experiment conducted with the treated activated carbon and 5.88 mol% THF showed multiple nucleation of the hydrate formation. The highest water conversion to the hydrates was achieved at 64.9 % in the system with H_2SO_4 treated activated carbon.

Keywords: Gas hydrate; Methane hydrate formation; Gas storage; Surface treatment; Activated carbon; Tetrahydrofuran

3.2 Introduction

Gas hydrates are crystalline, non-stoichiometric formed between water molecules and certain gas molecules under favorable conditions of pressure and temperature. In the hydrates, guest molecules like carbon dioxide, methane, and hydrogen are captured in the hydrate cages forming an ice-like framework. There are three common hydrate structures – sI, sII, and sH, which are known to form from a few types of hydrate cages, depending on the molecular size of the guest molecule and physical properties of the guest species (Englezos 1993; Sloan and Koh, 2008). For example, sI can host small molecules such as methane, ethane, and carbon dioxide, while sII can host larger molecules like propane and isobutene. Understanding the hydrocarbon hydrate formation and dissociation mechanisms in

porous media is of interest for natural gas storage and recovery.

In recent years, natural gas hydrates are expected not only to replace fossil fuels as a new energy source but also a means for natural gas storage and transportation (Sloan 2003; Ganji *et al.*, 2007; Kim *et al.*, 2011). Methane storage in the hydrate form has been investigated due to its large storage quantity. Methane hydrate of 1 m^3 yields an equivalent of 170 m^3 of methane gas at STP conditions or 0.55 m^3 of methane gas at 30 MPa (Englezos and Lee, 2005). Despite these advantages, storing methane in the hydrate form has been challenging due to the slow reaction between water and methane, the longer hydrate formation time, and the stability of the hydrates. (Kim *et al.*, 2011; Chari *et al.*, 2013).

It was reported that more than 70% of water can convert to hydrates for all the hydrate formation experiments that were performed in a water saturated silica sand matrix and contracted with methane at 8.0 MPa and 277.15 K (Linga *et al.*, 2009; Haligva *et al.*, 2010). Kim *et al.* (2011) demonstrated that the formation rate of methane hydrates increased by adding multi-walled carbon nanotubes (MWCNTs). Florusse *et al.* (2004) added tetrahydrofuran (THF) guest molecule (called promoter) to reduce the hydrogen hydrate formation pressure from 300 MPa at 280 K to 5 MPa at 279.6 K. The applicability of THF as a promoter for carbon dioxide capture from a flue gas was demonstrated by Linga *et al.* (2008) but they reported that, while the operating condition was lowered significantly, THF was found to slow down the reaction rates and gas consumption. The THF molecule readily occupies the large cages of sII forming a stable structure, which reduces the hydrogen storage capacity in the hydrates and the gas uptake rates. In addition, the oxidation by acid or alkali chemical can remove the mineral elements and increase the oxygen-containing groups on the surface of activated carbon such as phenolic group (–OH), lactone group (C=O), and carboxylic group (–COOH), leading to the hydrophilic on the surface of carbon (Shen *et al.*, 2008; Dai *et al.*, 2008; Li *et al.*, 2011). As methane hydrates form at the gas-liquid interface, it could be a suitable technique to increase the hydrate formation kinetics by increasing the adsorption of water on the activated carbon. Recently, Babu *et al.* (2013b) reported that the interstitial pore space and their connectivity played a key role in the methane hydrate formation in activated carbon. Based on a morphology study, Babu *et al.* (2013b) observed transient hydrate

formation and dissociation happening on an activated carbon particle in hydrate stability region.

The aims of this study was to improve the kinetics of methane hydrate formation in a fixed bed column by adding untreated and treated activated carbon, which were fully saturated with water. In addition, effects of adding THF were investigated. The experiments were carried out at 6 and 8 MPa at 277.15 K. The gas consumption, induction time, and water conversion to the hydrates were reported.

3.3 Experimental

3.3.1 Materials Preparation

Granular activated carbon (Carbokarn Co., Ltd., Thailand) was milled and sieved to 20 – 40 mesh size (400-841 micron). For activated carbon treatment, sulfuric acid (H_2SO_4, 98%, Lab-Scan, Thailand) and potassium hydroxide (KOH, Lab-Scan, Thailand) were used. Approximately, 25 g of the activated carbon were weighted and sonicated in 250 mL of 1 molar of acid and alkali solution for 45 min at 303 K. Then, the sample was washed adequately with deionized water until pH of the filtered water was 7 and dried at 393 K overnight in an oven. Ultra high purity methane (99.999 %, Labgaz Thailand Co., Ltd.) was used for the hydrate formation experiment. Tetrahydrofuran (THF, 99.8 %, Lab-Scan, Thailand) was used as received. The nitrogen adsorption analysis of the adsorbents was carried out using an Autosorp-1MP gas sorption system (Quantachrome Corporation) to examine the surface area, pore volume, and average pore diameter of activated carbon.

3.3.2 Apparatus

The schematic of gas hydrate apparatus is shown in Figure 3.1(a). It consisted of a high-pressure stainless steel crystallizer (CR) with an internal volume of 57.28 cm^3. There was a reservoir (R) with a volume of 50 cm^3. The crystallizer and reservoir were immersed in a cooling bath, and the temperature was adjusted and controlled using a controllable chiller. Two pressure transducers were employed to measure the pressure, with 0.13 % error (0–21 MPa). The temperature of the hydrate and gas phases in the crystallizer was measured using k-type thermocouples. Four

thermocouples were located inside the crystallizer at different positions: T1 at the top of the bed, T2 at the middle of the bed, T3 at the bottom of the bed, and T4 at the bottom of the crystallizer, as seen in Figure 3 1(b). A data logger was connected to a computer to record the data during the experiment.

3.3.3 Methodology

To study the effects of porous media on methane hydrate formation, approximately 13 g of water-saturated activated carbon were placed in the crystallizer for each experiment. For methane hydrate formation in pure water or THF solution, 30 mL of water or 5.88 mol% THF solution were added into the crystallizer. To eliminate air in the system, the crystallizer was vacuumed by a rotary vacuum pump. The crystallizer was then pressurized to the experimental pressure at 277.15 K. The data was then recorded every 10 s. All experiments were conducted in a batch manner (fixed amount of liquid and gas). During the hydrate formation, there was a pressure drop in the crystallizer due to gas consumption. The experiments were stopped when there was no further pressure drop.

Pressure and temperature data were used to calculate the methane consumption (moles of methane consumed) in the crystallizer. At any given time, the total number of moles of methane in the system, including CR and connecting tube, remained constant and equaled to that at time zero. Hence, the number of moles of the gas consumed for the hydrate formation at time t is given by equation 3.1;

$$\Delta n_{H,\downarrow} = n_{H,t} - n_{H,0} = \left(\frac{PV}{zRT}\right)_{G,0} - \left(\frac{PV}{zRT}\right)_{G,t} \tag{3.1}$$

where z is the compressibility factor calculated by Pitzer's correlation (Linga *et al.*, 2007; Babu *et al.*, 2013a). R is the universal gas constant. V is the volume of gas phase in the crystallizer. P and T are the pressure and temperature of the crystallizer. $\Delta n_{H,\downarrow}$ is the number of moles of gas consumed for the hydrate formation at the end of the experiment. $n_{H,t}$ is the number of moles of the hydrates at time t. $n_{H,0}$ is the number of moles of the hydrates at time zero. Subscripts of G,0 and G,t represent the gas phase at time zero and time t, respectively. In the presence of THF, the

conversion of water to hydrates was calculated with equation 3.2 (Veluswamy and Linga, 2013);

$$\text{Conversion (\%)} = \frac{(\Delta n_{H,\downarrow} + \Delta n_{THF}) \times \text{Hydration number}}{n_{H_2O}} \times 100 \quad (3.2)$$

where n_{H_2O} is the number of moles of water in the system. The hydration number is the number of water molecules per gas molecule. Δn_{THF} is the number of moles of THF consumed for the hydrate formation at the end of the experiment, which was calculated based on the assumption that THF occupied only the large cage of sII as seen in equation 3.3 (Veluswamy and Linga, 2013);

$$\Delta n_{THF} = \Delta n_{H,\downarrow} \times \frac{\text{number of large cages}}{\text{number of small cages}} \quad (3.3)$$

3.4 Results and Discussion

Table 3.1 summarizes 9 methane hydrate formation experimental conditions at 277.15 K, including initial pressure (experimental pressure), induction time, amount of gas consumption, and water conversion to hydrates. From Experiment 1 in the Table, there is no hydrate formation in the H_2O/CH_4 system until 48 hr, while Linga *et al.* (2012) observed the methane hydrate formation within 3 hr at the same condition. However, the hydrate formation rate and the water conversion to hydrate were very low. In the case of the H_2O/CH_4 system, the hydrate could form a thin film layer at the water-gas interface, which prevents the methane gas diffusion to liquid phase beneath the hydrate film at the interface for further hydrate growth (Linga *et al.*, 2012). This could be a reason why the hydrate formation was not observed with the experimental setup in this work.

3.4.1 Effect of Activated Carbon on the Methane Hydrate Formation

Figure 3.2 presents the gas uptake and temperature profiles during the methane hydrate formation of the untreated-AC/H_2O/CH_4 system at 8 MPa and

277.15 K. As seen in the figure, methane hydrates start to form rapidly after introducing methane gas into the system. Moreover, the induction time of each system listed in Table 3.1 indicates that the methane hydrates are formed at different times due to the stochastic nature of hydrate nucleation. These results are consistent as that reported by Linga *et al.* (2009), who reported that it might not be possible to predict the hydrate formation time. During the hydrate formation, heat is released due to the exothermic reaction, which can be seen in the temperature profiles in the figure. In addition, the first temperature increases in different positions of thermocouples were observed at same time because the methane hydrate may form at any position in the crystallizer, where activated carbon is saturated with water. Therefore, four thermocouples located at different positions inside the crystallizer are able to detect at the same time, as heat released during the methane hydrate formation as seen in Figures 3.2 and 3.3 in the experiment. The gas uptake increases gradually after the hydrate formation due to the hydrate crystal growth. It should be noted that the addition of the activated carbon enhances the methane hydrate formation by increasing the interstitial pore space or the contact area between water and gas, which results in the faster hydrate formation than the system without the activated carbon (Babu *et al.*, 2013b).

3.4.2 Effect of Treated Activated Carbon on the Methane Hydrate Formation

Figure 3.3 shows the gas uptake and temperature profiles during the methane hydrate formation of the H_2SO_4 treated-AC/H_2O/CH_4 system at 8 MPa and 277.15 K. After introducing methane gas into the crystallizer, the gas molecule starts to diffuse into water until it saturates and then forms hydrates at 83 min. That is evidenced by the sudden increase in the gas uptake and temperature spikes as clearly seen in the figure. The gas uptake and temperature profiles of this system are different from those of the untreated-AC/H_2O/CH_4 system in Figure 3.2. There are two steps of gas consumption after the hydrate formation, and the temperature spikes can be seen twice with the use of the treated activated carbon. This observation can be related to the formation of multiple nucleation events in the porous media and has been observed in the literature for silica sand as porous media (Linga *et al.*, 2009).

This behavior can also be observed in the system with KOH treated activated carbon. A possible reason could be the change in the functional groups on the surface of the activated carbon after the chemical treatment, especially oxygen-containing groups such as carboxylic group, phenolic group, and lactone group (Shen *et al.*, 2008; Dai *et al.*, 2008; Li *et al.*, 2011). Moreover, the cleaner surface and pore structure after the chemical treatment may also influence the gas consumption in the methane hydrate formation.

The comparison of the gas uptake profiles during the methane hydrate formation of the untreated and treated activated carbon at 8 MPa and 277.15 K is shown in Figure 3.4. As seen from the figure, the results show methane gas diffuses into the water and then forms hydrates at different induction times but the gas uptake profiles of the H_2SO_4 and KOH treated activated carbon show two steps of gas consumption. Although the hydrates form much faster in the system with the untreated activated carbon than that with the H_2SO_4 and KOH treated activated carbon, the system has much lower gas uptake. The system with the H_2SO_4 treated activated carbon shows the highest gas uptake followed by that with the KOH treated activated carbon.

Although there is no significant change in the BET surface area after the chemical treatment—867, 878, and 907 m^2/g for the untreated, KOH treated activated carbon, and H_2SO_4 treated activated carbon, respectively, the treatment must affect the surface chemical properties to a certain extent. It was reported that after H_2SO_4 treatment, the surface functional groups such as phenolic group (–OH), lactone group (C=O), and carboxylic group (–COOH) are increased compared with the untreated activated carbon, while the activated carbon treated by KOH contains lower carboxylic group and phenolic group but higher in the lactone group compared to the untreated activated carbon (Li *et al.*, 2011). The major increase takes place in the carboxylic group, which is due to the strong oxidation property of H_2SO_4 treatment (Li *et al.*, 2011). Moreover, Li *et al.* (2011) noticed a decrease in the phenolic group and an increase in the lactone group of the alkali treated activated carbon compared to the untreated activated carbon. As the result, the increase in the oxygen-containing group leads to the increase in the hydrophilic surface of activated carbon. In the case of methane hydrate formation, where the hydrates are initiated at

the gas-liquid interface, the possibility of water adsorbed on the carbon surface are increased, and results in the increase in the contact area and also the gas uptake on the methane hydrate formation. After introducing methane into the treated activated carbon, which is saturated with water, methane hydrates are formed and cover the surface and pore of the activated carbon. Over a period of time, the methane hydrates that cover the pore are cracked, and then the hydrates start to grow again inside the pore of the treated activated carbon (Jin *et al.*, 2012).

The results of the BET surface area indicate that, after the chemical treatment, the surface area is hardly changed from the untreated one. However, the impurities or small particles that cover the surface and pore wall of the activated carbon are removed after the treatment. Therefore, the two-step gas consumption as seen in Figures 3.3 and 3.4 could be caused by the increase in the hydrophilic surface of the treated activated carbon and the impurity removal, while this mechanism is not observed in the untreated activated carbon because the impurity and small particles cover the surface or block the pore, and also the lower oxygen-containing group than the activated carbon treated by H_2SO_4 and KOH. In addition, no methane hydrate formation was observed in the untreated-AC/H_2O/CH_4 system within 48 hr after attaining the pressure at 6 MPa as shown in Table 3.1. On the contrary, the treated-AC/H_2O/CH_4 system, both treated by H_2SO_4 and KOH, can form the hydrates at the low pressure (6 MPa) but the conversion of water to hydrate is lower than that at the high pressure (8 MPa).

Figure 3.5 shows the hydrate growth profiles during the methane hydrate formation in 60 min. As seen from the figure, the gas consumption or hydrate growth of all experiments increase gradually during the first 60 min before reaching the steady state. The H_2SO_4 treated activated carbon shows the highest hydrate growth followed by the KOH treated activated carbon and untreated activated carbon at 8 MPa, respectively. It should be noted that the chemical treatment of activated carbon could improve the methane hydrate growth for the hydrate formation by increasing the surface oxygen-containing groups of activated carbon and removing the impurities from the activated carbon.

3.4.4 Effect of THF on the Methane Hydrate Formation

Figure 3.6 shows the gas uptake and temperature profiles during the methane hydrate formation with the presence of 5.88 mol% THF at 8.1 MPa and 277.15 K conducted without the activated carbon. As seen form the figure, the hydrates form very fast, within 10 min, and there are several temperature spikes after the first nucleation. The positions of thermocouple inside the crystallizer indicate that the hydrates start forming at the interfacial surface of the THF solution and goes down to the bottom. The gas uptake increases suddenly at the beginning due to the first hydrate nucleation, and again before reaching the steady state. This observation can only be seen when the hydrate formation takes place in the presence of the THF solution at 6.1 MPa and 8.1 MPa. Prasad *et al.* (2009) also observed the methane/THF mixed hydrate with different THF concentrations ranging in 5.88 to 1.46 mol%.

The unit cell structure of THF hydrates is structure II (sII) with eight large cages occupied by THF molecules, while sixteen small cages are vacant and could possibly be occupied by methane molecules in mixed methane/THF hydrates (Chari *et al.*, 2012). Therefore, the presence of THF in the system can form THF hydrate and also induce methane molecules to form methane hydrate in the small cages of sII. Considering the experiment 8 (8.1 MPa) in Table 3.1, the total water conversion is 53.2%, which consists of 72% methane hydrate and 28% THF hydrate. Methane/THF hydrate fraction is also the same in experiment 9 (6.1 MPa). This result indicated that the fraction of methane hydrate and THF hydrate does not depend on the experimental pressure.

According to Table 3.1, the methane hydrate formation kinetics of the H_2O/CH_4 system is low at 8 MPa as evidenced by no hydrate formation within 48 hr. The increase in the contact area between the gas molecule and water by adding the treated and untreated activated carbon into the system results in the increase in the hydrate growth. However, with the activated carbon, decreasing the pressure from 8 to 6 MPa results in no hydrate formation within 48 hr (Experiment 3). In addition, the presence of THF and H_2SO_4 and KOH treated activated carbon can improve the kinetics of the hydrate formation at 6 MPa.

3.5 Conclusions

The effects of activated carbon and THF on the kinetics of hydrate formation were demonstrated. At 8 MPa, the addition of the untreated activated carbon enhanced the kinetics of the hydrate formation, while adding activated carbon treated by H_2SO_4 and KOH increased the gas consumption during the methane hydrate formation and the hydrate formation kinetics at 6 MPa by increasing the surface oxygen-containing groups of the activated carbon. Similarly, the presence of THF solution also improved the hydrate formation kinetics at the low pressure (6 MPa) conducted without the activated carbon. The experiment conducted by the treated activated carbon and 5.88 mol% THF showed the multiple nucleation (observed by temperature spikes and gas uptake). The water conversions to the hydrates in the range of 25.1–64.9 % were achieved.

3.6 Acknowledgments

This study was supported by The Royal Golden Jubilee Ph.D. Program (2.P.CU/51/J.1), Thailand Research Fund; The Petroleum and Petrochemical College (PPC), Chulalongkorn University, Thailand; National Metal and Materials Technology Center (MTEC), Thailand; Center of Excellence on Petrochemical and Materials Technology (PETROMAT), Thailand; Ratchadaphisek- somphot Endowment Fund of Chulalongkorn University (RES560530021-CC); UOP, A Honeywell Company, USA.

3.7 Nomenclature

$\Delta n_{H,\downarrow}$ = number of moles of methane gas consumed for hydrate formation

$n_{H,t}$ = number of moles of the hydrates at time t

$n_{H,0}$ = number of moles of the hydrates at time zero

G,0 = gas phase at time zero

G,t = gas phase at time t

Δn_{THF} = number of moles of THF consumed for hydrate formation

n_{H_2O} = number of moles of water

V_{CR} = volume of the gas phase of the crystallizer, cm^3

z = compressibility factor

R = universal gas constant, $cm^3 \cdot MPa \cdot K^{-1} \cdot mol^{-1}$

P = pressure, MPa

T = temperature, K

BET = The multipoint Brunauer, Emmett, and Teller method used to measure the total surface area

3.8 References

Babu, P., Kumar, R., and Linga, P. (2013a) Pre-combustion capture of carbon dioxide in a fixed bed reactor using the clathrate hydrate process. Energy, 50, 364-373.

Babu, P., Yee, D., Linga, P., Palmer, A., Khoo, B.C., Tan, T.S., and Rangsunvigit, P. (2013b) Morphology of methane hydrate formation in porous media. Energy Fuels, 27, 3364-3372.

Chari, V.D., Sharma, D.V.S.G.K., Prasad, P.S.R., and Murthy, S.R. (2013) Methane hydrates formation and dissociation in nano silica suspension. Journal of Natural Gas Science and Engineering, 11, 7-11.

Chari, V.D., Sharma, D.V.S.G.K., and Prasad, P.S.R. (2012) Methane hydrate phase stability with lower mole fractions of tetrahydrofuran (THF) and *tert*-butylamine (*t*-$BuNH_2$). Fluid Phase Equilibrium, 315, 126-130.

Dai, X.D., Liu, X.M., Zhao, G., Qian, L., Qiao, K., and Yan, Z.F. (2008) Treatment of activated carbon for methane storage. Asia-Pacific Journal of Chemical Engineering, 3, 292-297.

Englezos, P. (1993) Clathrate hydrates. Industrial & Engineering Chemistry Research, 32, 1251-1274.

Englezos, P. and Lee, J.D. (2005) Gas hydrates - a cleaner source of energy and opportunity for innovative technologies. Korean Journal of Chemical

Engineering, 22(5), 671-681.

Florusse, L.J., Peters, C.J., Schoonman, J., Hester, H.C., Koh, C.A., Dec, S.F., Marsh, K.N., and Sloan, M.E. (2004) Stable low-pressure hydrogen clusters stored in a binary clathrate hydrate. Science, 306, 469-471.

Ganji, H., Manteghian, M., and Mofrad, H.R. (2007) Effect of mixed compounds on methane hydrate formation and dissociation rates and storage capacity. Fuel Processing Technology, 88, 891-895.

Haligva, C., Linga, P., Ripmeester, J.A., and Englezos, P. (2010) Recovery of methane from a variable-volume bed of silica sand/hydrate by depressurization. Energy Fuels, 24, 2947-2955.

Jin, Y., Konno, Y., and Nagao, J. (2012) Growth of methane clathrate hydrates in porous media. Energy Fuels, 26, 2242-2247.

Kim, N.J., Park, S.S., Kim, H.T., and Chun, W.A. (2011) Comparative study on enhanced formation of methane hydrate using CM-95 and CM-100 MWCNTs. International Communications in Heat and Mass Transfer, 38, 31-36.

Li, L., Liu, S., and Liu, J. (2011) Surface modification of coconut shell based activated carbon for the improvement of hydrophobic VOC removal. Journal of Hazardous Materials, 192, 683-690.

Linga, P., Adeyemo, A., and Englezos, P. (2008) Medium-pressure clathrate hydrate/membrane hybrid process for postcombustion capture of carbon dioxide. Environmental Science & Technology, 42, 315-320.

Linga, P., Daraboina, N., Ripmeester, J.A., and Englezos, P. (2012) Enhanced rate of gas hydrate formation in a fixed bed column filled with sand compared to a stirred vessel. Chemical Engineering Science, 68, 617-623.

Linga, P., Haligva, C., Nam, S.C., Ripmeester J.A., and Englezos, P. (2009) Gas hydrate formation in a variable volume bed of silica sand particles. Energy Fuels, 23, 5496-5507.

Linga, P., Kumar, R., and Englezos, P. (2007) Gas hydrate formation from hydrogen/carbon dioxide and nitrogen/carbon dioxide gas mixtures. Chemical Engineering Science, 62, 4268-4276.

Prasad, P.S.R., Sowjanya, Y., and Prasad, K.S. (2009) Micro-raman investigation of

mixed gas hydrates. Vibrational Spectroscopy, 50, 319-323.

Shen, W., Li, Z., and Liu, Y. (2008) Surface chemical functional groups modification of porous carbon. Recent Patents on Chemical Engineering, 1, 27-40.

Sloan, E.D. (2003) Fundamental principles and applications of natural gas hydrates. Nature, 426, 353-359.

Sloan, E.D. and Koh, C.A. (2008) Clathrate hydrates of natural gases. (3rd ed. (pp 45-72). New York: CRC Press.

Veluswamy, H.P. and Linga, P. (2013) Macroscopic kinetics of hydrate formation of mixed hydrates of hydrogen/tetrahydrofuran for hydrogen storage. International Journal of Hydrogen Energy, 38, 4587-4596.

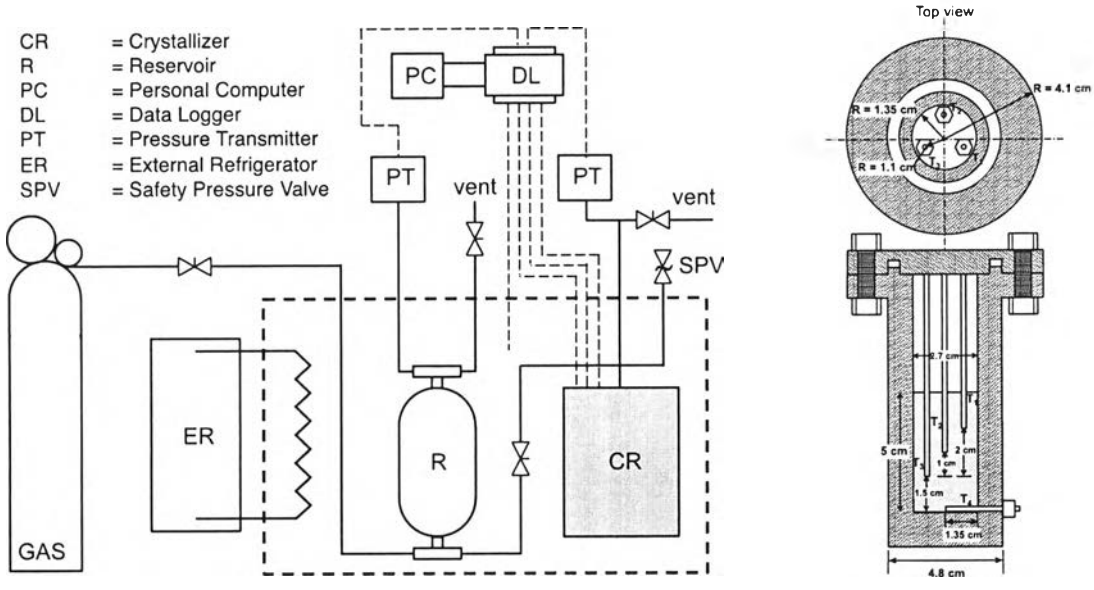

(a) (b)

Figure 3.1 Gas hydrate apparatus; a) schematic diagram, b) cross-section of a crystallizer.

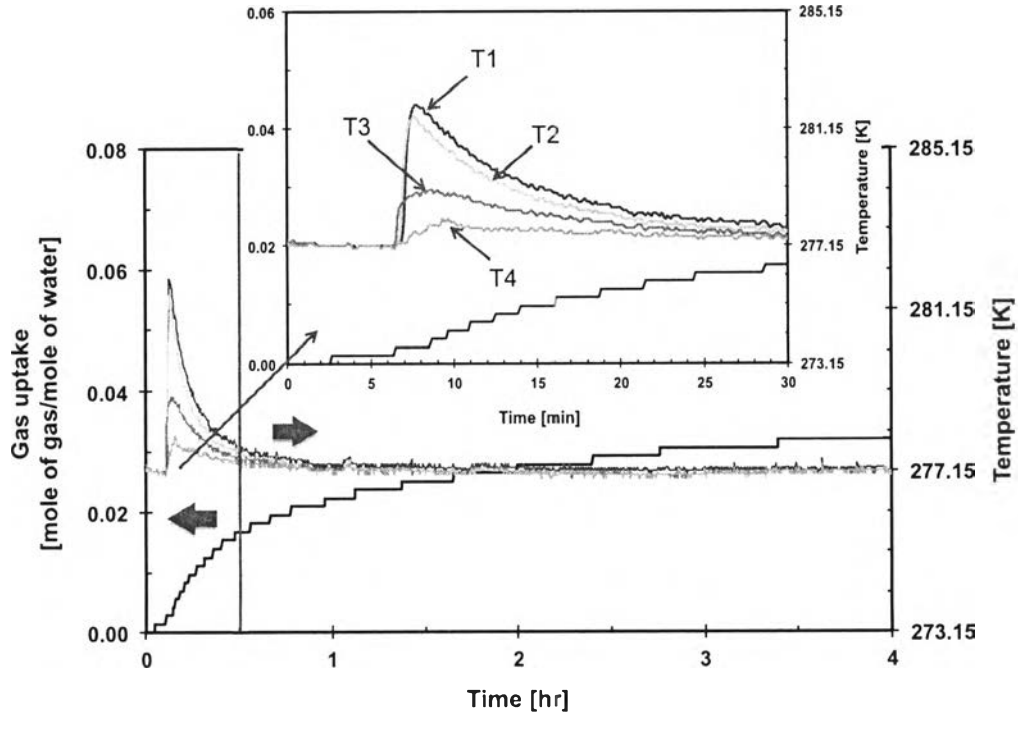

Figure 3.2 Gas uptake and temperature profiles during the methane hydrate formation of the untreated-AC/H_2O/CH_4 system at 8 MPa and 277.15 K (Experiment 2).

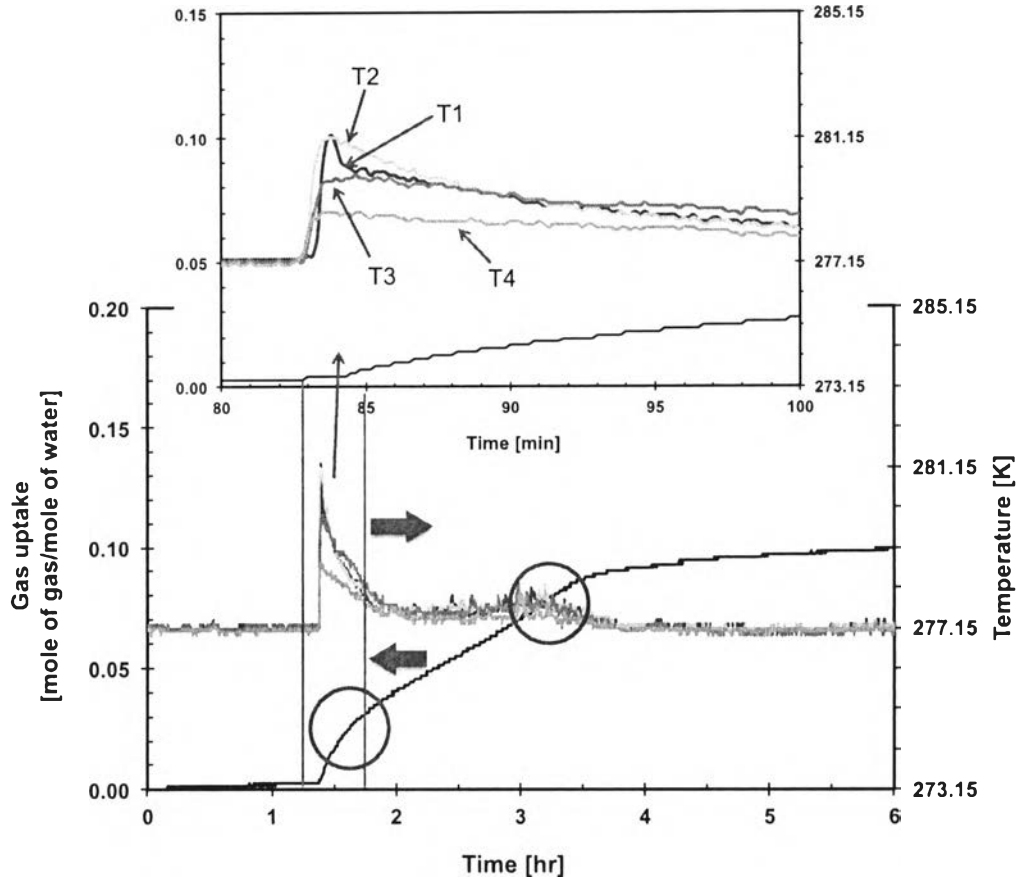

Figure 3.3 Gas uptake and temperature profiles during the methane hydrate formation of the H_2SO_4 treated-AC/H_2O/CH_4 system at 8 MPa and 277.15 K (Experiment 4).

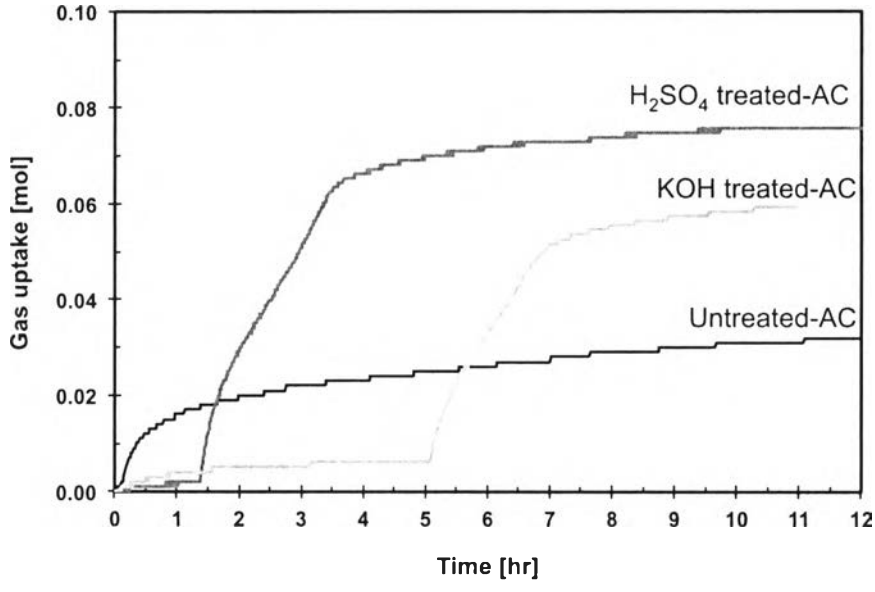

Figure 3.4 Comparison of gas uptake profiles during the methane hydrate formation of the untreated-AC/H_2O/CH_4 system (Experiment 2), H_2SO_4 treated-AC/H_2O/CH_4 system (Experiment 4), and KOH treated-AC/H_2O/CH_4 system (Experiment 6) conducted at 8 MPa and 277.15 K.

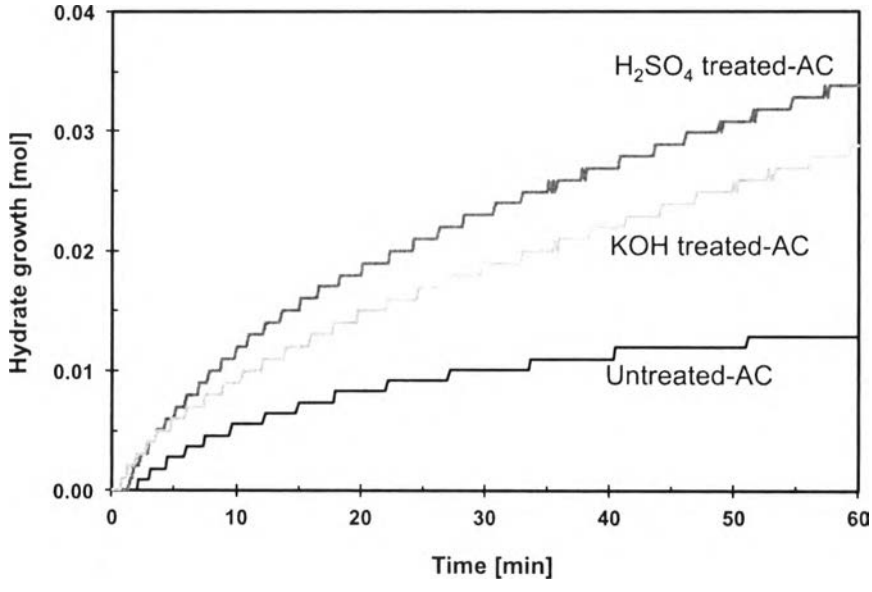

Figure 3.5 Comparison of hydrate growth profiles during the methane hydrate formation in the presence of untreated-AC (Experiment 2), H_2SO_4 treated-AC/H_2O/CH_4 (Experiment 4), and KOH treated-AC/H_2O/CH_4 (Experiment 6) in 60 min at 8 MPa and 277.15 K (Time zero in the graph corresponds to the induction time listed in Table 3.1).

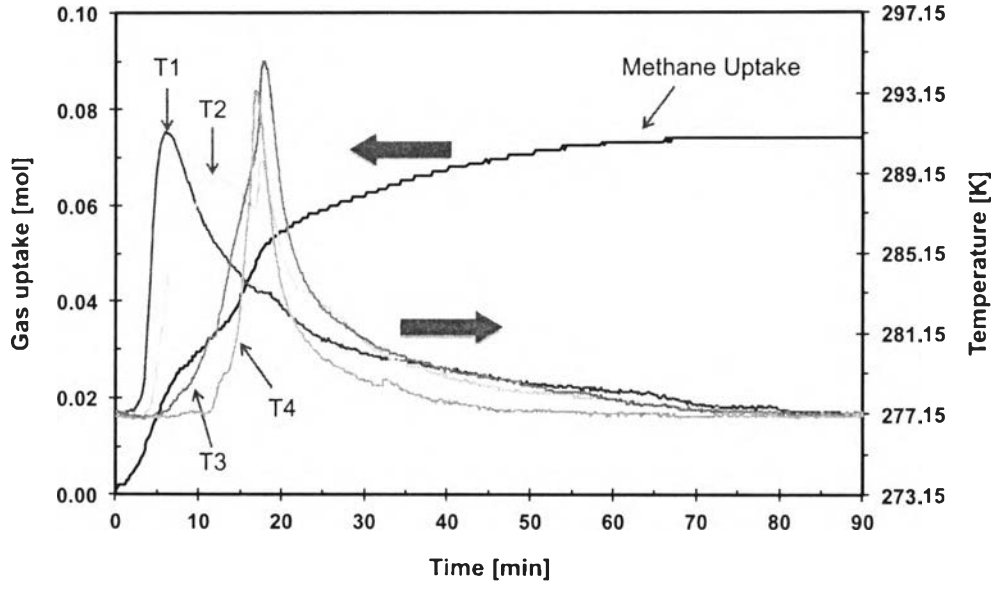

Figure 3.6 Gas uptake and temperature profiles during the methane hydrate formation with the presence of 5.88 mol% THF at 8.1 MPa and 277.15 K (Experiment 8).

Table 3.1 Hydrate formation experimental conditions at 277.15 K

Expt No.	System	Initial pressure (MPa)	Induction time (min)*	End of experiment		Water conversion to hydrate (mol%)**/(Avg./SD)***
				Time (hr)	CH_4 consumed (mol/mol of H_2O)	
1	H_2O/CH_4	8.0	NHF til 48 hr	-	-	-
2	Untreated-AC/H_2O/CH_4	8.0	6.8	21.7	0.0511	31.2/(33.9/4.28)
3	Untreated-AC/H_2O/CH_4	6.0	NHF til 48 hr	-	-	-
4	H_2SO_4 treated-AC/H_2O/CH_4	8.0	83	13	0.1064	64.9/(66.2/6.31)
5	H_2SO_4 treated-AC/H_2O/CH_4	6.0	826	20.2	0.0412	25.1/(29.0/4.55)
6	KOH treated-AC/H_2O/CH_4	8.0	305.5	11	0.0822	50.1/(54.1/3.59)
7	KOH treated-AC/H_2O/CH_4	6.0	355.2	14.8	0.0412	25.1/(26.6/3.28)
8	5.88mol%THF/CH_4	8.1	4.2	4.4	0.0627	53.2/(56.3/3.43)
9	5.88mol%THF/CH_4	6.1	5.7	14	0.0550	46.7/(48.1/3.35)

NHF = No Hydrate Formation

*Induction time is the first hydrate formation.

**Water conversion to hydrates (%) was calculated using Equations (3.2) and (3.3) with the hydration number of 6.1 for Experiments 1–7 and 5.66 for Experiments 8–9.

***Avg. = Average and SD = Standard Deviation